45th Aerospace Sciences Meeting, January 8-11, 2007, Reno, Nevada

Modification of the Flow Structure over a UAV Wing for Roll Control

Robert C. Nelson,[*] Thomas C. Corke,[†] Chuan He,[‡] Hesham Othman[§] and Takashi Matsuno[¶]
University of Notre Dame, Notre Dame, IN 46556

Mehul P. Patel[‖] and T. Terry Ng[**]
Orbital Research Inc., Cleveland, OH 44103

Plasma enhanced aerodynamics was used to provide roll control at high angles of attack on a scaled 1303 UAV configuration. The 1303 planform has a 47 degree leading-edge sweep angle. The flow over the a half-span model was documented with dye flow visualization in a water tunnel for a range of angles of attack. This revealed a complex flow structure that varied with angle of attack. A half-span model with Single Dielectric Barrier Discharge (SDBD) plasma actuators was then tested in a wind tunnel. The model was mounted on a 2-D force balance designed to measure lift and drag. At larger angles of attack from 10 to 35 degrees, plasma actuators placed just below the leading edge were found to augment the lift. This configuration was implemented in a full-span model that was mounted on a sting that allowed free-to-roll motion. The ability of the plasma actuator arrangement to produce roll maneuvers was then investigated for a range of angles of attack and free-stream speeds. The results indicated excellent roll control with roll moment coefficients that are comparable to conventional moving surfaces.

I. Introduction

In the past decade active flow control concepts of various types have been developed that can successfully improve the aerodynamic characteristics of lifting surfaces. These early studies clearly showed that flow control actuators could delay stall thereby increasing the stall angle of attack and maximum lift of the lifting surface.[1,2] More recently researchers have been looking at applying active flow control to create aerodynamic control moments.[3] One such project is currently underway as a joint research venture between Orbital Research Inc. and the University of Notre Dame. The goal of this research program is to develop a flying wing that uses active flow control technology to create aerodynamic control moments of sufficient magnitude so that conventional moving aerodynamic controls could be eliminated.

The quest for efficient flow-control for improved vehicle aerodynamics has led to the design and development of many ingenious flow-control actuators and control techniques over the years. It is becoming increasingly clear however, for a flow-control actuator to make its way onto an air vehicle, it not only needs to demonstrate an ability to generate forces necessary for flight control, but also an overall improvement in the aerodynamic and structural efficiencies of the vehicle (relative to the conventional control system). While a majority of the flow-control research has focused largely on lift enhancement through separation control over two-dimensional wings, the present work explores the control of the longitudinal and lateral dynamics of a

*Professor, Fellow AIAA.
†Clark Chair Professor, Associate Fellow AIAA.
‡Ph.D. Candidate
§Post-doctoral Associate
¶Visiting, Tottori University, Japan
‖Director, Aerodynamics Group, Senior Member, AIAA.
**Senior Member, AIAA.

highly three-dimensional, 47-deg leading-edge sweep geometry. The UAV configuration chosen for this study is based on an Air Force-Boeing Phantom Works 1303 UAV design. A photograph showing the planform of the 1303 design is shown in Figure 1. The vehicle is basically a blended wing body where the fuselage is blended smoothly with the wing with a varying cross-section along the span and $\pm 30°$ trailing-edge sweep angle. The design of the 1303 UAV features conventional (hinged) flap and split-ailerons for aerodynamic control.

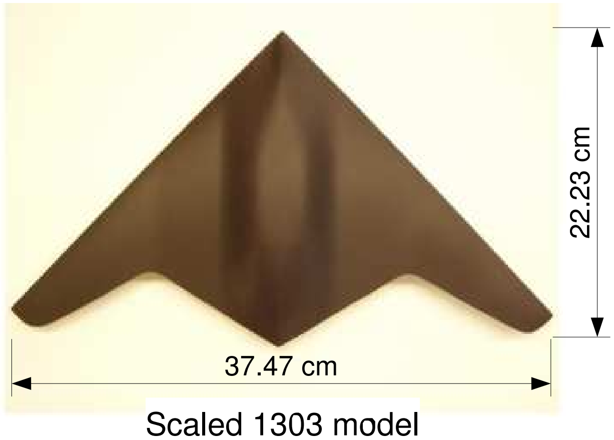

Figure 1. Photograph showing plan view of scale 1303 full-span model used for free-to-roll experiments.

Swept wings of low aspect ratio are commonly used on high-speed aircraft because of their favorable wave drag characteristics. Leading edge vortex (LEV) is the main feature of the flow over swept wings which provide lift for flight control at high angles of attack. At low angles of attack and lower speeds however, the aerodynamic behavior of swept wings is vastly different than the high-aspect ratio wings. The performance of swept wings outside the high-speed high-alpha envelope is crucial as the mission roles of modern aircraft required them to operate at low-speed and low-alpha conditions during various flight phases (e.g., take-off, landing). The formation of the LEV and subsequent vortex break down (VBD) phenomena over a swept wing are highly influenced by a number of parameters including angle of attack, leading-edge design, adverse pressure gradients, which present unique challenges in controlling the vehicle dynamics at different flow conditions. For example, at low angles of attack, the flow remains attached to the surface and the location of the (weak) VBD is usually downstream within the wake of the wing. As the angle of attack increases, the strength of the LEV increases and the location of VBD begins to move forward. The VBD phenomenon is usually associated with a loss in vortex lift, which has been shown to cause changes in the lift, drag, and pitching moments of the swept wing vehicle. At large angles of attack, the upper wing surfaces show the presence of complex vortex systems which dominate the upper flowfield, and cause the wing tip separations.

In the past decade, several researchers have employed flow-control methods to control the LEV and VBD phenomena for improved aerodynamics of a swept wing. For example, Moeller and Rediniotis[4] demonstrated control of the pitching moment of a 60-deg sweep delta wing model at high angles of attack using a series of surface-mounted pneumatic vortex control actuators. Control was achieved by altering the vortex breakdown phenomena which affected the chord-wise lift distribution over the wing, ultimately resulting in an induced pitching moment. Amitay *et al.*[5] reported an experimental study on the use of synthetic jet actuators on a 1301 UAV design (nicknamed "Stingray"). The design of Stingray and the present 1303 UAV share some similarity, in that the leading-edge sweep-angle is approximately 50 degrees, leading to similar three-dimensional flow patterns over the wing. Amitay *et al.*[5] showed that at conditions where the flow was normally separated from the leading-edge, between 14 and 24 degrees angles of attack, the zero-mass jets were able to produce forces and moments on the vehicle. Visser and Nelson[6–8] employed steady spanwise blowing to control leading-edge vortex breakdown and asymmetric roll-moment conditions.

In a more recent effort, a computational study on the aerodynamic performance of a 1303 UAV design for different leading-edge designs was reported by Zhang *et al.*[9] The effects of three leading-edge designs: a basic profile, a rounded leading-edge (similar to the one used in our study), and a sharp leading-edge were investigated using the NPARC code at a Mach number of 0.25, and at angles of attack ranging from -5 to 20 degrees. It was found that there were only minor differences among pressure distributions with the three configurations for both the computed and experimental data. The predicted pressure distributions compared favorably with their wind tunnel measurements for all regions except near the wing tips where the computations did not consistently predict the observed flow separations. At small angles of attack, flowfield studies showed attached, smooth and well-behaved flow.

The flying wing aircraft that have been developed and successfully flown rely on multiple control surfaces distributed across the wing to provide control moments for trim and maneuvering. Each control surface is essential a trailing edge flap that when deflected changes the lift, drag and pitching moment over that portion of the wing. By suitably arranging multiple flaps across the wing one can create moments to pitch, roll, or yaw the wing as well as moments to trim the wing at a particular flight condition.

The ultimate objective of the present work is to demonstrate hingeless flight control with limited or no use of conventional control surfaces. This paper presents results using Single Dielectric Barrier Discharge (SDBD) plasma actuators placed near the leading edge to provide roll control at high angle of attack flight conditions.

II. Experimental Setup

A series of experiments were performed in three facilities at the University of Notre Dame using two different scale models of the 1303 planform. These experiments began with flow visualization in a water tunnel that were used to characterize the flow at different angles of attack. Following this, lift and drag measurements were performed on a half-span model in air to access the optimum locations of plasma actuators for lift control. Although these involved plasma actuators at the leading and trailing edges, only the results with the leading-edge actuators are reported here. Finally a full-span model was used to examine the ability of the plasma-based flow control to provide roll control at large angles of attack. Details of the three experimental setups are presented in the following sections.

A. Flow Visualization

Flow visualization was performed using a half-span model in a water tunnel. Photographs of the half-span model are shown in Figure 2. The half span model had a root chord of 16 inches (40.64 cm) and a half-span dimension of 13.375 inches (13.97 cm). The models were cast from a numerically machined two-piece aluminum mold. The casting material is a mixture of epoxy and micro glass beads that results in a very rigid model that accurately duplicates the mold shape.

The water tunnel at the University of Notre Dame is an Eidetics design having a test section with a width of 15 inches (38.1 cm), a height of 18 inches (45.7 cm) and a length of 6 ft (1.8 m). Different color flow tracer dyes were used to visualize the flow over the wing surface. Four dye ports were incorporated into the half span model, two ports were located on the leeward surface and two were located on the windward surface. The leeward side ports that were located near the apex of the wing, and all of the the windward ports, were located at $b/8$ and $b/4$ (where b is the equivalent full wing span), and at 10% of the chord from the leading edge. The flow visualization photographs were obtained as a function of angle of attack. The angle of attack was varied from 0 to 20 degrees in two degree increments. The Reynolds number for the water experiments was 3.5×10^4 based on the root chord.

B. Half-span Lift Setup

Lift and drag measurements on the half-span model were conducted in the 1.5 foot (45.72 cm) square cross-section open-return wind tunnel at the University of Notre Dame. The test section length is 6 ft (1.8 m). The turbulence level in the test section is $u'/U_\infty = 0.08\%$.

The half-span model was mounted vertically on the support sting of a lift-drag force balance that was mounted on the top of the test section. A schematic of the force balance and the test section is shown in Figure 3. The model was suspended below a splitter plate that was attached to the ceiling of the test section. The splitter plate was designed to produce a two-dimensional flow with a thin boundary layer leading up to the model. A hole in the ceiling splitter plate accommodated the sting supporting the model. Wiring for

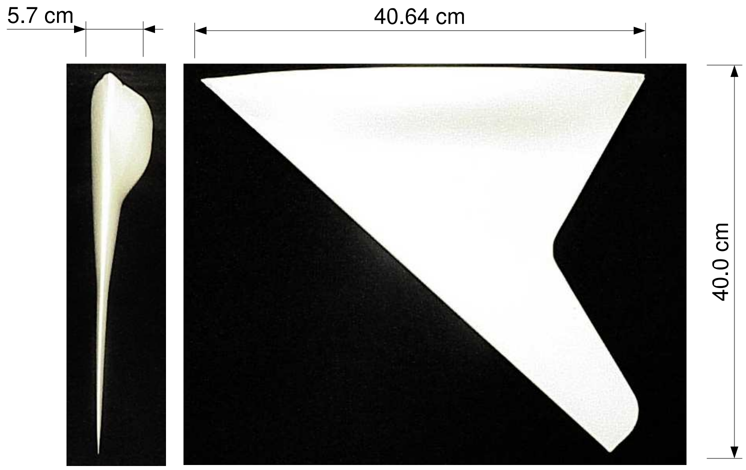

Figure 2. Photographs showing two views of scale 1303 half-span model used for dye flow visualization and lift-drag measurements with SDBD plasma actuator.

the plasma actuator also entered through this hole. A stepper motor on the force balance drove the angular position of the support sting. Its motion was controlled by the data acquisition computer through software.

The force balance consists of independent lift and drag platforms. The lift platform is supported on the drag platform by two vertical plates that flex only in the lift direction. The drag platform is supported by two plates that flex only in the drag direction and hang from two more vertical plates attached to the fixed base of the force balance. Both the lift and drag platforms are connected to separate flexures on which foil strain-gauge bridges are mounted. The strain-gauge bridges provide voltage outputs proportional to the respective lift and drag forces. The voltages were amplified using custom designed operational amplifier circuits that minimized offset drift and sensitivity to external electronic noise. Calibration of the force balance was done by applying known weights to a cable pulley system attached to the support sting.

The experiment was controlled by a digital computer with a programmable analog-to-digital (A/D) converter and digital input-output (DIO) interface. The minimum voltage resolution of the A/D converter was 0.6 mV. The voltages proportional to the lift and drag forces were acquired along with a voltage proportional to the velocity at the entrance to the test section. The acquisition software was programmed to acquire 10,000 voltage samples over 10 seconds. This was found to provide repeatable time averaged statistics that varied by less than 0.1 percent.

The angular position of the airfoil was controlled by voltage pulses from the DIO into the stepper motor controller. With this, the angular position was repeatable to within ± 0.005 degrees. A mechanical readout that was geared to the stepper motor shaft provided positive feedback on the angular position.

Prior to making lift-drag measurements, values of the lift and drag voltages were first acquired at different angles of attack <u>without flow</u>. Any difference from the zero force voltages that was due to eccentric loading was then recorded and subtracted from the results at the same angles of attack with flow. This process was repeated any time the model was removed from the force balance.

The free-stream speed at the entrance to the measurement section was measured with a pitot-static probe connected to a pressure transducer. The output of the transducer was monitored on a d.c. volt meter and simultaneously acquired by the data acquisition computer when the voltages proportional to the lift and drag forces were acquired. Based on the pressure transducer calibration, the accuracy of the free-stream speed measurements was 0.01 m/s. The combination of the uncertainties in the force measurements and velocity resulted in an average uncertainty in the lift and drag coefficients of approximately 1 percent.

The measurements were primarily performed at a free-stream speed of 15 m/s. Based on the root chord, this corresponded to $Re_c = 4.12 \times 10^5$.

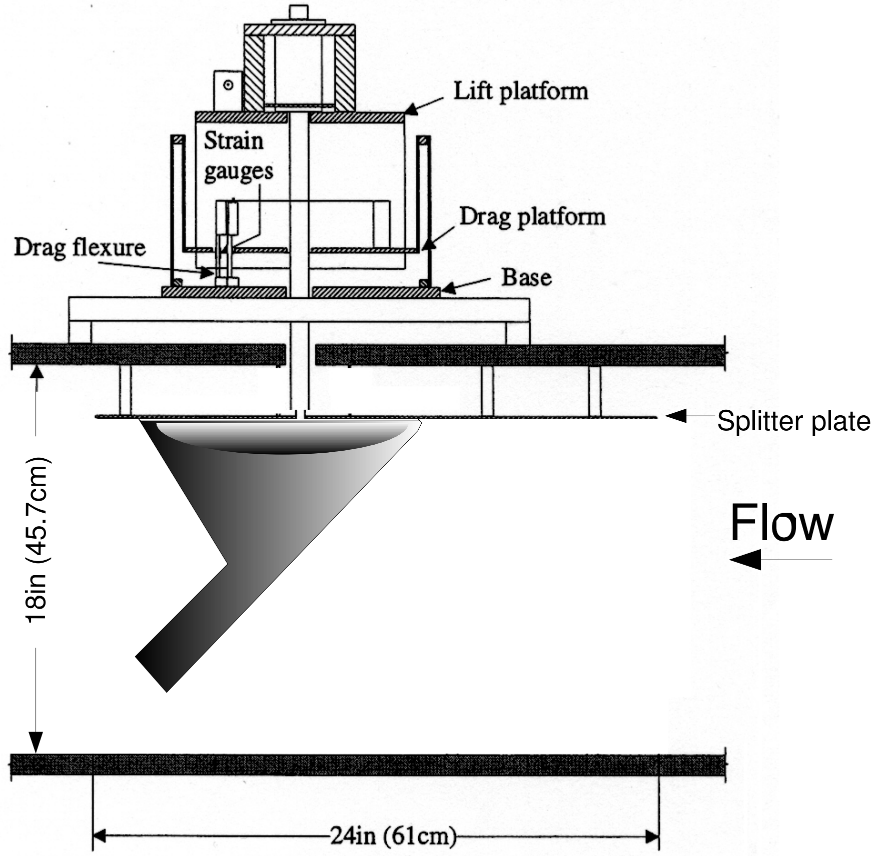

Figure 3. Schematic of half-span model mounted on two-component force balance in wind tunnel.

C. Full-span Free-to-roll Setup

The ability of the plasma actuator arrangement to produce roll maneuvers was investigated with a full-span model in a 2 foot (60.96 cm) square cross-section open-return wind tunnel at the University of Notre Dame. The test section length is 6 ft (1.8 m). The turbulence level in the test section is $u'/U_\infty = 0.08\%$. The model used was that previously shown in Figure 1. For this as noted in the figure, the wing span was 14.75 inches (37.47 cm) and the root chord was 8.85 inches (22.23 cm).

The model was mounted on a sting that was held with low-friction roller bearings to allow roll motion. A schematic of the setup is shown in Figure 4. The bearings were mounted to a plate that was located below the tunnel floor. The plate could be rotated to place the model at different angles of attack, α. A GMW360ASM angular position sensor was mounted at the base of the sting. This used a magnetic coupling so that it did not induce any angular moment on the sting. The output from the angular position sensor was a voltage proportional to the angular position. This voltage was acquired by the data acquisition computer through one of the A/D channels. The accuracy of the angular motion detector was $\pm 1^\circ$ and the response time is $\leq$ 5ms.

The bearing plate holding the model sting was located in an enclosure below the test section floor. The enclosure was sealed so that it was at the same static pressure as the test section. The model sting entered the test section through a slot at the spanwise centerline of the tunnel floor.

Photographs of the full-span model in the test section are shown in Figure 5. These show the location of the electrodes that make up the SDBD plasma actuator. The arrangement of the actuator was the same as that found to produce the best change in lift at high angles of attack in the half-span measurements.

The free-to-roll experiments were conducted at a range of free-stream speeds from 10 to 30 m/s and angles of attack from 10 to 35 degrees. For these velocities the Reynolds number based on the root chord ranged from 1.50×10^5 to 4.50×10^5. Note that the higher Reynolds number closely matches that of the half-span lift-drag experiments.

The amplitudes of the plasma actuators on each half wing span were initially adjusted so that when operated simultaneously, the wing tips were level. The data acquisition computer was programmed to independently turn the two actuators on and off in any combination and for any duration. The roll response of the model as measured by the angular motion sensor, which was simultaneously recorded by the data acquisition computer.

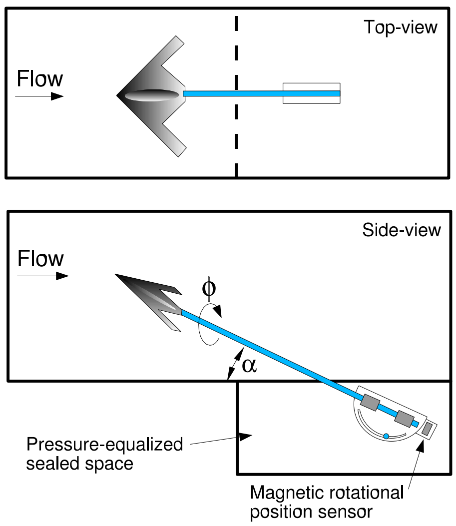

Figure 4. Schematic of full-span model mounted on a sting that allowed free roll motion.

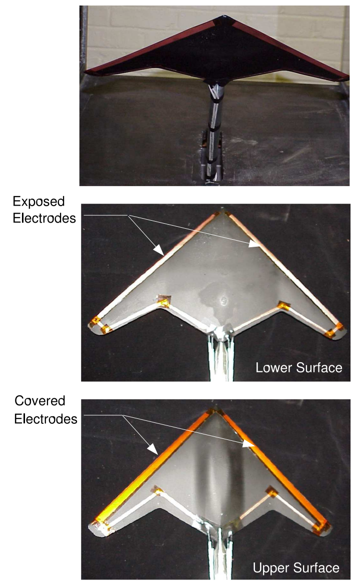

Figure 5. Photographs of full-span model mounted on a sting that allowed free roll motion.

D. Plasma Actuators

The plasma actuators consisted of two copper electrodes separated by two layers of 0.002 inch (0.05 mm) thick Kapton film. The electrodes were made from 0.001 inch (0.0254 mm) thick copper foil tape. The electrodes were arranged in the asymmetric arrangement illustrated in Figure 6. They were overlapped by a small amount (of the order of 0.5 mm), in order to ensure a uniform plasma in the full spanwise direction. A high voltage alternating current (a.c.) input was supplied to the electrodes. When the a.c. voltage amplitude was large enough, the air ionized in the region over the covered electrode. This is shown by blue in the illustration.

The process of ionizing the air in this configuration is classically known as a single dielectric barrier discharge.[10] The ionized air (plasma) in the presence of an electric field gradient produces a body force vector that acts on the ambient air.[11] With this arrangement of electrodes, the body force produced by the actuator would induce a velocity component in the direction from the exposed electrode towards the covered electrode. With it oriented as shown on the wing, it induces a flow around the leading edge.

The plasma actuator was bonded directly to the surface of the airfoil. The two copper foil electrodes were aligned parallel with the leading edge. The spanwise length of the actuators was 90 percent of the wing span. The exposed electrode on the lower side of the model can be seen in the middle photograph in Figure 5. The electrode covered by the Kapton film can be seen on the upper side of the model in the lower photograph in Figure 5.

The a.c. frequency of the input voltage supplied to the electrodes was typically 5 kHz. The a.c. voltage amplitude to the electrodes was 7.5 kV$_{p-p}$. In all the cases, the actuator was switched off and on at a lower frequency, f, such that the dimensionless frequency, $F^+ = f\bar{c}/U_\infty$, was unity, where $\bar{c}$ is the mean

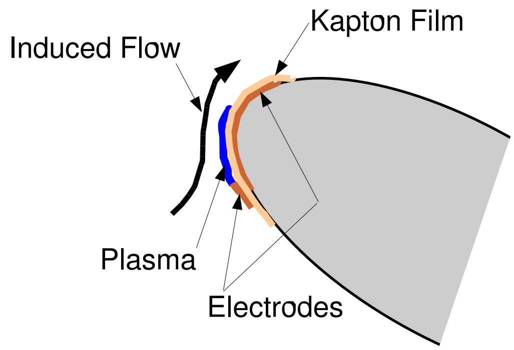

Figure 6. Example of electrode arrangement for SDBD plasma actuator for full span model. Note thicknesses are exaggerated for clarity.

aerodynamic chord. Previous measurements[3] had shown that this results in the optimum conditions to re-attach separated leading-edge flows on wings.

III. Results

The results are presented in chronological order of the experiments. This begins with flow visualization which documents the basic features of the flow over the wing at different angles of attack. The flow visualization results guided the design and placement of the plasma actuators. The results of the lift-drag measurements with the plasma actuators documented the optimum arrangement to maximize the change in lift. The results presented here focus on the leading edge actuators which were effective at larger angles of attack. Finally the result of the lift-drag experiments were used to design the free-to-roll experiment.

A. Flow Visualization

The objective of the flow visualization experiments was to to understand the flow structure over the 1303 wing so that the locations of flow actuators could be optimized to maximize their control moments. A sample of the flow visualization records are shown in Figure 7. The photographs show the dye patterns on the upper surface of the 1303 model as a function of angle of attack. At lower angles of attack, $\alpha \leq 7°$, the dye patterns indicate that the flow over most of the upper surface is dominated by a mean cross-flow from the wing root towards the tip. At these angles of attack, trailing edge flow control devices (conventional moving or other) can be effective. One possible problem occurs over the outboard tip wing panel where the dye pattern indicates that a reverse flow exists. The left photograph in Figure 8 illustrates this.

At larger angles of attack, $\alpha > 8°$, the dye patterns indicate the formation of a leading edge vortex. At $\alpha = 8°$, the vortex appears to persist in length along the leading edge to approximately b/4 in span. As the angle of attack increases, vortex breakdown moves toward the wing apex as expected. The right photograph in Figure 8 corresponds to $\alpha = 12°$ where the extent of the leading edge vortex is particularly evident. Here, the leading edge vortex appears to break down near the break in the trailing edge sweep angle, where the diffused dye downstream of breakdown spreads both inboard and over the outboard panel.

B. Half-span Lift Measurements

A series of experiments were performed to evaluate the effectiveness of plasma actuators to provide flight control on the 1303 planform. These experiments used the same scale half-span model as the flow visualization experiments. The results presented were for a free-stream velocity of 15 m/s, where $Re_c = 4.12 \times 10^5$.

The results presented here deal only with flight control using leading edge plasma actuators. Based on the flow visualization, these were expected to be most effective at larger angles of attack, $\alpha \geq 8°$. Our previous work[3] indicated the optimum location for separation control on 2-D wing sections was directly at the leading edge. Therefore that was a starting point. In terms of spanwise locations for the actuator, the wing span was

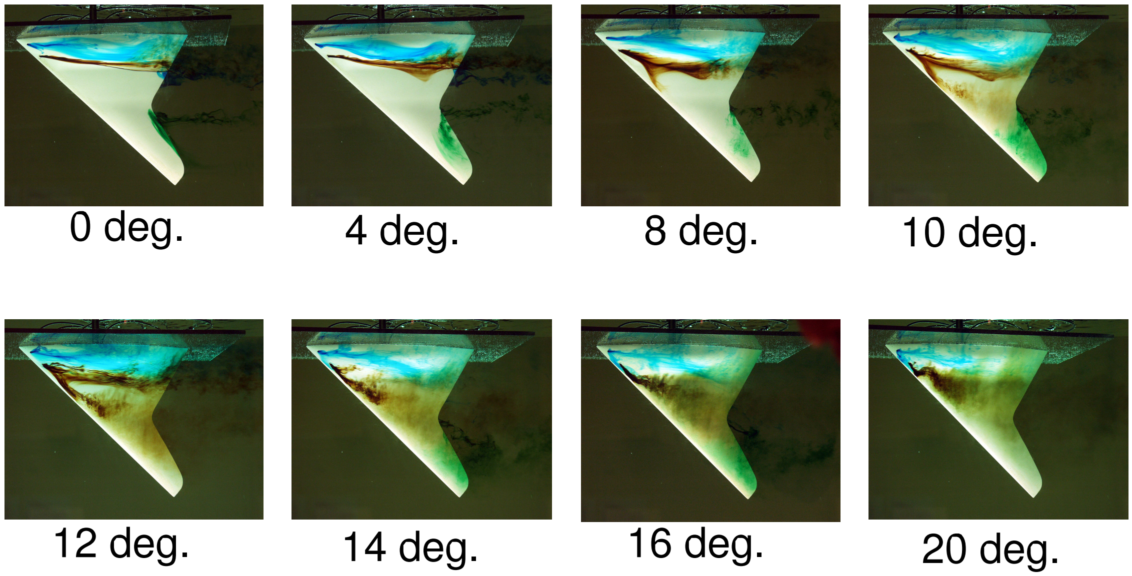

Figure 7. Visualization records of the flow over the upper surface of the half-span 1303 UAV model for a range of angles of attack. $Re_c = 3.5 \times 10^4$

divided into two equal length regions, one being the inboard half span, and the other being the outboard half span. The actuators in these two regions were individually controllable in order to document their effect on lift augmentation. A schematic that shows the four leading-edge actuator configurations is shown in Figure 9. The left column corresponds to an actuator placed at the exact leading edge ($x/c = 0$). The right column corresponds to the actuator placed on the lower surface, slightly downstream of the leading edge ($x/c \simeq 0.03$). The rows indicate the spanwise locations of the actuator. The top row corresponds to the inboard location, $0.08 \geq y/b \geq 0.55$. The bottom row corresponds to the outboard location, $0.56 \geq y/b \geq 0.99$.

The flow visualization indicated that at higher angles of attack ($> 8°$) the wing was dominated in the inboard span by a leading-edge vortex, and in the outboard span by a leading-edge flow separation. Therefore we focus on the two span regions separately.

Figure 10 compares the lift coefficient versus angle of attack for the two leading edge actuator positions at the inboard span location. At this span location, the effect of the actuator only occurs at angles of attack that are greater than 19 degrees. For these, the actuator placed on the pressure side just below the leading edge ($x/c \simeq 0.03$) had more of an effect on the lift.

Figure 11 compares the lift coefficient versus angle of attack for the two leading edge actuator positions at the outboard span location. The actuators at this span location show an effect on the lift for a much larger range of angles of attack than the inboard actuators. In this case the lift is increased over the base case from 9° up to the largest angle, 35°. As with the inboard actuators, the actuator placed on the pressure side just below the leading edge ($x/c \simeq 0.03$) had more of an effect on the lift.

Based on these results, the plasma actuator on the full-span free-to-roll model were located on the lower surface of the wing at $x/c \simeq 0.03$. However in contrast to the half-span model experiments, a single actuator that spanned each wing was used. Based on the lift measurements, the greatest effect would come from the control of the outboard span flow separation. The outboard panel would also contribute most to the roll moment. However we were interested in achieving the maximum roll moment, and for $\alpha \geq 20°$, the inboard portion of the actuator would contribute.

C. Full-span Free-to-roll Measurements

A series of experiments were conducted to evaluate the effectiveness of the plasma actuators to produce a roll moment for controlling the roll attitude of the 1303 UAV model at high angles of attack. As noted earlier, flow visualization showed that the flow over the outboard panels of the wing was completely separated at

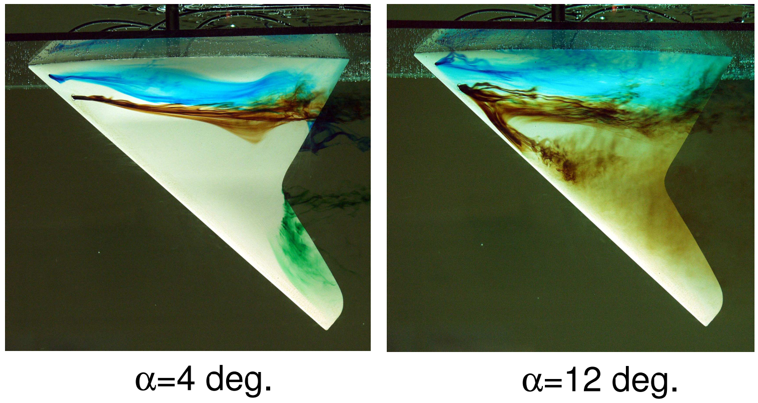

Figure 8. Enlarged visualization records of the flow over the upper surface of the half-span 1303 UAV model at $\alpha = 4°$ (left) and $12°$ (right). $Re_c = 3.5 \times 10^4$

large angles of attack. Therefore leading-edge flow actuators offered the best opportunity to re-attach the flow for lift enhancement and roll control, in the high angle of attack regime.

The model was free to roll about the longitudinal axis as was depicted in Figure 4. Without flow control the model was statically unstable in roll at large angles of attack, $\alpha \geq 10°$, and would roll to either a positive or negative equilibrium bank angle. This is most likely due to any non-uniformity in the outboard flow regions. Any small spanwise asymmetry in the flow separation over the outboard panels would cause the wing to be unstable at zero bank angle.

As mentioned, the right and left wing actuators extended from the wing centerline to the wing tip. In the initial experiments presented here the voltage signal to the left and right wing actuators were cycled in a manner shown in Figure 12 for $U_\infty = 15$ m/s and $\alpha = 20°$.

In Figure 12, when both actuators were turned on, the model maintained a zero bank angle, $\phi = 0°$. Turning off the right wing actuator caused the model to rapidly roll right to a trim point near, $\phi = -40°$[a]. Then when the left wing actuator was turned off and the right wing actuator was turned on, the model rolled rapidly to the left, to a new trim angle at $\phi = +40°$. Finally when both wing actuators were turned on, the model rolled back to the original zero bank angle, $\phi = 0°$. Figure 13 shows repeated programmed control cycles for the same angle of attack and velocity as Figure 12. This illustrates that the roll control was completely repeatable.

The effect of increasing tunnel speed on the programmed roll motion is shown in Figure 14. In this case, $\alpha = 20°$ and the free-stream speed ranges from 10 to 30 m/s. The programmed wing actuator cycle was identical to that in Figure 12. Figure 14 documents the roll motion trajectories as the actuators are cycled through the sequence: both off, both on, left on - right off, both on, left off-right on, both off.

The magnitude of the roll excursion is still approximately $\pm 40°$. The major difference we observe between the roll response curves is that the model tends to oscillate more about the trim angle as the free-stream speed increases. This is most likely due to the larger roll moment produced on the model at the higher velocities. The oscillation is more apparent when the left actuator is on. Without static roll data and aerodynamic damping measurements it is difficult to offer a complete explanation of the response trajectories. Nevertheless these experiments clearly show that the leading edge plasma actuators can be used to provide roll control at large angles of attack.

One method used to investigate the roll motion response of the model due to the wing actuators involved forced roll oscillations. For this, the actuators were cycled on and off at different frequencies. Figure 15 shows time history plots of the forced oscillation for frequencies of 3.3, 2 and 1.0 Hertz. As would be expected, the magnitude of the oscillation increased as the actuation frequency is lowered.

Figure 16 is comparable to Figure 15 but with a faster free-stream speed. Also as expected, the magnitude of the oscillations increased with the increase in the free-stream speed because of the larger aerodynamic

[a]The sign is opposite to the standard convention

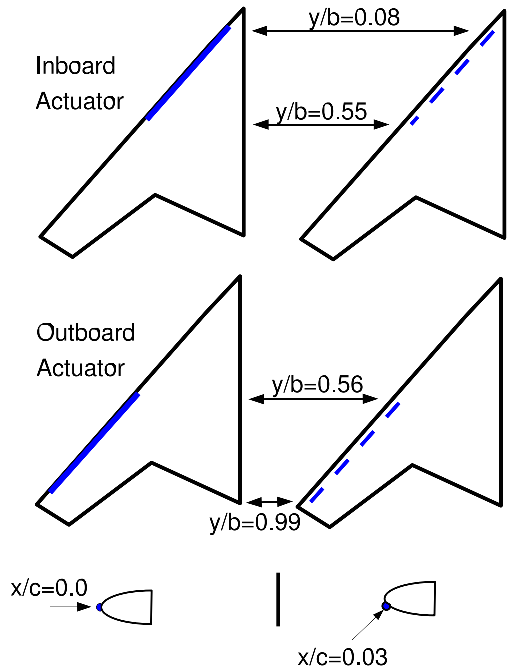

Figure 9. Schematic showing the four leading-edge actuator configurations that apply to the results presented.

loads and resulting control authority. We also note in both of the forced roll oscillation cases that the roll motion was not symmetric about the zero bank angle at the higher frequencies. The degree of bias was comparable at both free-stream speeds. Further experiments will be needed to understand this behavior. However, these experiments have clearly shown that leading edge plasma actuators can provide a roll control capability on the 1303 planform that is very responsive.

D. Conventional Aileron Comparison

The free-to-roll experiments showed that the plasma actuators on the leading edge of the outboard wing panel could produce a control moment to rotate the model on the free to roll support system. The roll moment was not measured in our experiment, so a simple analysis is presented here to give the reader a feel for the effectiveness of the roll capability of the plasma actuators.

An estimate of the roll coefficient was made using the information shown Figure 17. The roll moment is due to the change in lift created by plasma actuators on the outboard wing panel given as

$$\mathcal{L} = \Delta C_L q S_a r_a$$

which gives a roll moment coefficient of

$$C_{\mathcal{L}} = \frac{\mathcal{L}}{q S_w b} = \frac{(\Delta C_L) S_a r_a}{S_w b}$$

where ΔC_L is the change in the wing lift coefficient produced by the actuator, q is the free-stream dynamic pressure, S_a is the area of the wing affected by the plasma actuator, r_a is the distance of the center of lift in the affected area S_a, and S_w and b are the wing area and span used in normalization. Using this information, with ΔC_L taken from Figure 11, a roll moment coefficient of $C_{\mathcal{L}} = 0.0044$ was found.

To put the roll moment coefficient produced by the leading-edge plasma actuator in perspective, another calculation was made to estimate the roll moment coefficient that would be produced by conventional ailerons at the trailing edge of the same wing planform. These are indicated in Figure 17. The characteristics of the ailerons are $C_a/C = 0.2$, $\delta_a = \pm 20°$, and a flap effectiveness factor of $\tau = 0.4$. For this arrangement, the

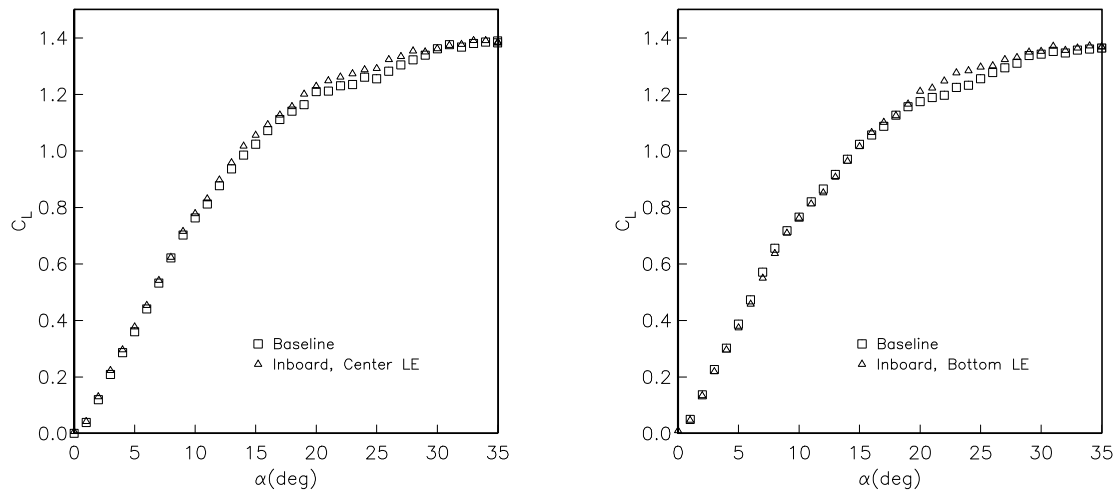

Figure 10. Lift coefficient versus angle of attack at the inboard span location for the two leading edge actuator positions, $x/c = 0$ (left) and lower-surface-$x/c \simeq 0.03$ (right).

maximum moment coefficient produced by the conventional trailing-edge ailerons at a maximum deflection angle ($\delta_a = 20°$) was $C_{\mathcal{L}} = 0.0040$. Thus the plasma actuator was as effective as the conventional aileron for roll control.

It is important to point out that the maximum moment coefficient due to the conventional ailerons was for a low angle of attack where they are most effective. They would become ineffective at the high angles of attack where the leading edge plasma actuators were operated. On the other hand, the leading-edge plasma actuators used for roll control are only effective at the higher angles of attack ($> 8°$). This is not a problem for employing plasma actuators for control. For example, separate trailing-edge plasma actuators have been investigated on the 1303 planform[12,13] to replace conventional ailerons for flight control at low angles of attack.

IV. Conclusions

The flow over the suction surface of a scaled 1303 UAV model was found to be highly three-dimensional. At lower angles of attack, $\alpha \leq 7°$, the dye flow patterns indicate that the flow over most of the upper surface was dominated by a mean cross-flow from the wing root towards the tip. At these angles of attack, trailing edge flow control devices (conventional moving or other) could be effective with the exception of the outboard tip wing panel where the dye patterns indicates that a reverse flow exists. At larger angles of attack, $\alpha > 8°$, the dye patterns showed the formation of a leading edge vortex. The vortex appeared to persist in length along the leading edge to approximately one-quarter span of the wing. Under these high angle of attack conditions, trailing-edge flow control devices will not be very effective, and flight control is best performed by leading-edge devices.

Single Dielectric Barrier Discharge (SDBD) plasma actuators located near the leading edge of the 1303 wing were found to be very effective in controlling the lift in the high angle of attack regime. Optimum lift enhancement was found by placing the actuators at a chordwise location that was close to the leading edge on the suction side at $x/c \simeq 0.03$. The actuators were placed parallel to the leading edge. For these, the actuator on the inboard half of the wing was only effective for angles of attack greater than 20 degrees. The actuator on the outboard half of the wing was however effective for angles of attack from 9° up to the largest angle examined, 35°.

When this arrangement of leading edge plasma actuators was installed on a full-span free-to-roll 1303 model, it was found to provide excellent roll control capability that was very responsive. This was demonstrated for a range of angles of attack from 10 to 30 degrees and free-stream speeds from 10 to 30 m/s which gave a chord Reynolds number range from 1.50×10^5 to 4.50×10^5.

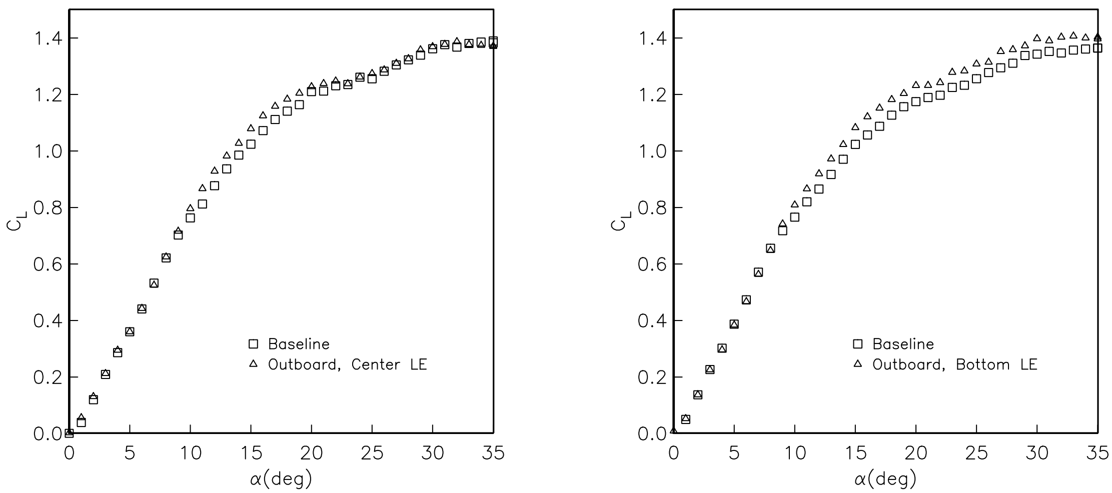

Figure 11. Lift coefficient versus angle of attack at the outboard span location for the two leading edge actuator positions, $x/c = 0$ (left) and lower-surface-$x/c \simeq 0.03$ (right).

Analysis of the roll control produced by the plasma actuators to those of conventional trailing edge ailerons showed them to have identical roll moment coefficients. Thus the plasma actuator was as effective as a conventional aileron for roll control.

Acknowledgment

This work was supported as a subcontract from Orbital Research Inc. as part of a SBIR Phase II contract from the USAF/AFRL, WPAFB under Contract Number FA8650-04-C-3405. The USAF program manager is Dr. Charles Suchomel. The U.S. Government is authorized to reproduce and distribute reprints for government purposes not withstanding any copyright notation therein.

References

[1]Post, M., "Plasma Actuators for Separation Control on Stationary and Oscillating Wings." Ph.D. Dissertation, University of Notre Dame, 2004.

[2]Post, M. and T. Corke, "Separation control on high angle of attack airfoil using plasma actuators", AIAA Journal, Vol. 42, No. 11, pp. 2177, 2004.

[3]Corke, T. C., He, C. and Patel, M., "Plasma flaps and slats: an application of weakly-ionized plasma actuators", 2nd AIAA Flow Control Conference, AIAA Paper 2004-2127, Accepted *AIAA J.*, 2004.

[4]Moeller, E.B. And Rediniotis, O. K., "Hingeless Flow Control Over a Delta Wing Platform", AIAA Paper No. 2000-117.

[5]Amitay, M. Washburn, A.E., Anders, S. G. and Parekh, D., "Active Flow Control on a Stingray Uninhabited Air Vehicle: Transient Behavior", AIAA J. Vol. 42, No. 11, Nov., 2004.

[6]Visser, K.D., "An Investigation of the Effects of an External Jet on the Performance of a Highly Swept Delta Wing", M.S. Thesis, University of Notre Dame, 1988.

[7]Visser, K.D., Nelson, R.C., and Ng, T.T., "A Flow Visualization and Force Data Evaluation of Spanwise Blowing on Full and Half Span Delta Wings," AIAA-89-0192, AIAA 27th Aerospace Sciences Meeting, January 9-12, 1989 Reno, NA.

[8]Visser, K.D., Iwanski, K.P., Nelson, R.C., and Ng, T.T., "Control of Leading Edge Vortex Breakdown by Blowing," AIAA-88-0504, AIAA 26th Aerospace Sciences Meeting, January 11-14, 1988 Reno, NV.

[9]Zhang, F. Khalid, M., and Ball, N. "A CFD Based Study of UCAV 1303 Model," AIAA Paper No. 2005-5615.

[10]Enloe, L., McLaughlin, T., VanDyken, R., Kachner, K., Jumper, E., and Corke, T., "Mechanisms and Response of a Single Dielectric Barrier Plasma Actuator: Plasma Morphology," *AIAA J.*, **Vol 42**, No.3, 2004, pp. 589-594; Also *AIAA 2003-1021*.

[11]Enloe, L., McLaughlin, T., VanDyken, R., Kachner, K., Jumper, E., Corke, T., Post, M., and Haddad, O., "Mechanisms and Response of a Single Dielectric Barrier Plasma Actuator: Geometric Effects," *AIAA J.*, **Vol 42**, No. 3, 2004, pp. 585-604.

[12]Lopera, J., Ng, T., Patel, M., Vasudevan, S., and Corke, T.. "Aerodynammic control of 1303 UAV using windward surface plasma actuators on a separation ramp," 45th Aerospace Sciences Meeting, AIAA Paper 2007-0636, 2007.

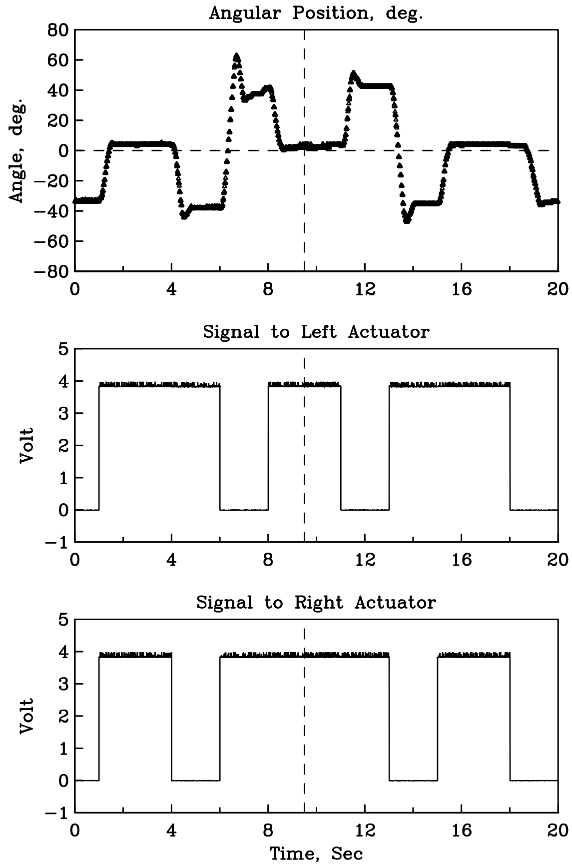

Figure 12. Response of free-to-roll model due to a programmed left and right wing plasma actuator schedule. $U_\infty = 15$ m/s and $\alpha = 20°$.

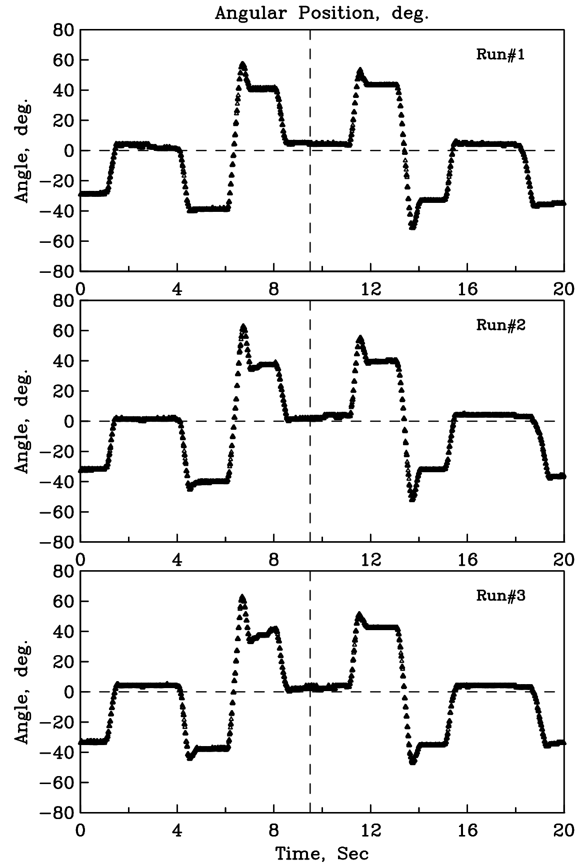

Figure 13. Three realizations of the response demonstrating the repeatability of free-to-roll motion due to the programmed left and right wing plasma actuator schedule shown in Figure 12. $U_\infty = 15$ m/s and $\alpha = 20°$.

[13]Patel, M. P., Ng, T. T., Vasudevan, S., Corke, T. C., and He, C., "Plasma Actuators for Hingeless Aerodynamic Control of an Unmanned Air Vehicle," AIAA Paper 2006-3495, 3rd AIAA Flow Control Conference, June 2006.

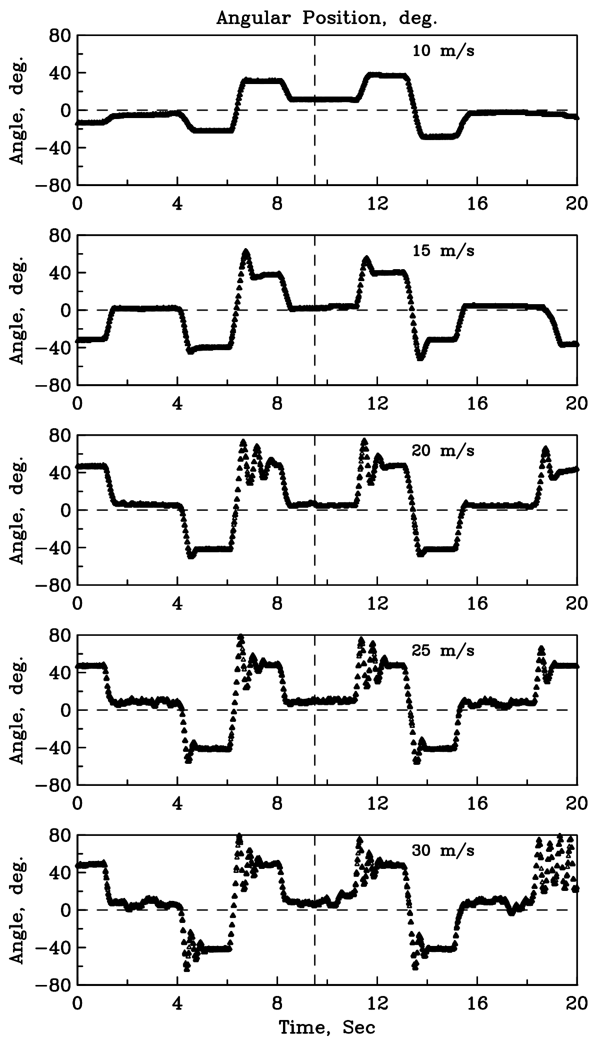

Figure 14. Response of free-to-roll model due to the programmed left and right wing plasma actuator schedule shown in Figure 12 for different free-stream speeds at $\alpha = 20°$.

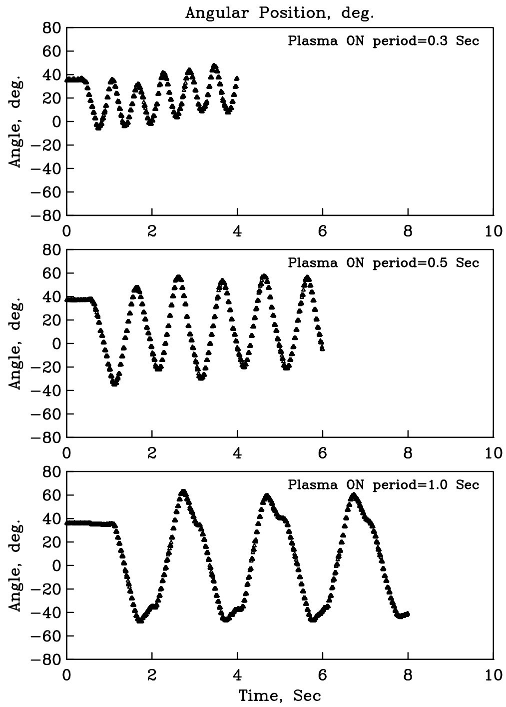

Figure 15. Response of free-to-roll model due to the programmed cyclic left and right wing plasma actuator to produce frequencies of 3.3, 2 and 1 Hz. $U_\infty = 15$ m/s and $\alpha = 20°$.

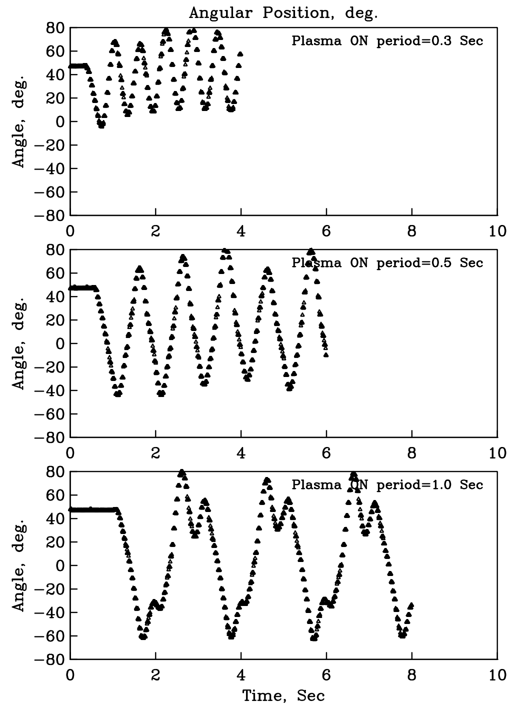

Figure 16. Response of free-to-roll model due to the programmed cyclic left and right wing plasma actuator to produce frequencies of 3.3, 2 and 1 Hz. $U_\infty = 20$ m/s and $\alpha = 20°$.

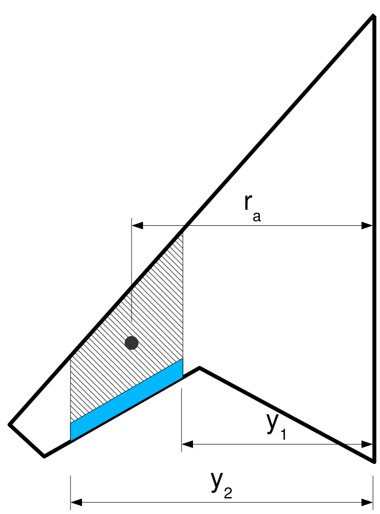

Figure 17. Schematic of conventional trailing-edge aileron used in comparison to leading-edge plasma actuator effect on roll. Note $C_a/C = 0.2$.